Supplementary information for "Heinrich Events: unpacking the convoluted freshwater connection"

Kevin Hank[1,2*], Matthew Drew[1] and Lev Tarasov[1]

[1*]Department of Physics and Physical Oceanography, Memorial University of Newfoundland, St. John's, NL, Canada.

[2]Natural Environment Research Council, British Antarctic Survey, High Cross, Madingley Road, Cambridge, CB3 0ET, United Kingdom.

*Corresponding author(s). E-mail(s): khank@mun.ca;
Contributing authors: mdrew@mun.ca; lev@mun.ca;

S1 Full model domain

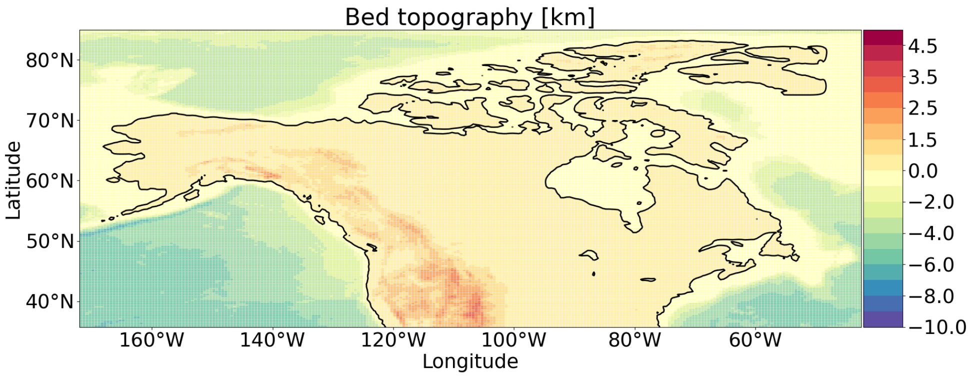

Fig. S1 GSM input present-day bed topography for the full model domain. The black contour line shows the present-day sea level (coastline) used in the GSM. Note the change in the color bar step at 0 km.

S2 Revised ice-rafted debris volume estimates

The Heinrich Layer thickness estimates in this study are based on Table 1 in [1]. The thickness estimates can vary significantly between different studies, even when examining the same layer in the same core. The causes of such differences are multifaceted but are generally related to the definition of a Heinrich Layer and the methods used. For example, Heinrich Layer 2 in core *CH69-K09* (lat = 41.75°N, lon = 47.35°W) has sediment thickness estimates of 3 and 62 cm [1, and references therein].

In a first step, we replace duplicate entries with the average sediment thickness (32.5 cm in the above case). We then remove all cores that do not provide a sediment thickness estimate for any of the 6 Heinrich Layers (note that the data includes 0 cm thickness estimates). Finally, we calculate the mean sediment thickness ($d_{\mathrm{sed,mean}}$) in all remaining cores (ignoring Heinrich Layers for which no thickness estimate is available). However, we also calculate a sediment volume estimate for each Heinrich Layer individually.

While we do not consider the above difference of 59 cm to be representative of the general uncertainty of Heinrich Layer thickness estimates (for the same layer and core), differences of 5 to 10 cm occur frequently [1, and references therein]. To incorporate this uncertainty and provide lower/upper bounds, we use the minimum/maximum sediment layer thickness in each core and further subtract/add 10 cm ($d_{\mathrm{sed,min}}/d_{\mathrm{sed,max}}$). However, we ensure the sediment thickness is at least 1 cm ($\min[d_{\mathrm{sed,mean}}] = 1.5$ cm).

To estimate the total sediment volume transported during a HE, we interpolate the sediment thickness between the core locations. The interpolation grid covers the area between 37.8°N to 61.5°N and 58.7°W to 9.5°W (∼ min/max lat/lon core location; black box in Fig. 2) with a latitudinal and longitudinal increment of 0.1°. To bound the data set and extract a more realistic sediment distribution, we added 8 data points with 0 cm sediment thickness at the minimum and maximum latitudinal extent (magenta circles in Fig. 2). Various different interpolation methods are available. Here we compare the piecewise-linear, nearest-neighbor, Clough-Tocher [all provided by the Python module *SciPy* version 1.5.2, 2], and ordinary kriging [Python module *PyKrige* version 1.7.2, 3] interpolation schemes.

Negative values from the Clough-Tocher and ordinary kriging interpolation are replaced by 0 m sediment thickness in a post-processing step. Integrating the interpolated sediment thickness over the interpolation area yields the final sediment discharge volume estimate.

Heinrich Layer sediment thickness estimates assume that all of the sediment between the interpreted top and bottom of a Heinrich Layer in a core is IRD. In sediment cores close to Hudson Strait – with the thickest Heinrich Layers – this is unlikely [4–6]. While the percentage of IRD during HEs is generally above 80 %, it can be as low as 40 % for some events and cores [Fig. 1 in 1]. Therefore, our revised IRD volume estimates are more accurately an upper bound for the actual IRD volume. Different methods for identifying and quantifying IRD [7] as well as diagenesis and dissolution after deposition – leading to underestimation of IRD volume – further complicate the interpretation.

For an average Heinrich Layer, the sediment discharge volume estimates between different interpolation methods vary significantly (Fig. 2, S2 to S4, and Table S1). Due to large areas with thick sediment in 3 corners of the interpolation area (Fig. S2), the nearest-neighbor scheme yields the largest estimates. Piecewise-linear and ordinary kriging interpolation slightly reduce the estimates, but the Clough-Tocher method returns the smallest estimates. Overall, the sediment discharge volume estimates (based on mean, minimum, and maximum sediment thickness estimates) vary between 187 and 2078 km^3, with a mean of 981 ± 699 km^3 (± indicates the standard deviation, Table S1).

Table S1 Revised IRD volume estimates for an average and individual Heinrich Layers using different interpolation methods. The average, minimum, and maximum estimates are based on the sediment thickness estimates $d_{\mathrm{sed,mean}}$, $d_{\mathrm{sed,min}}$, and $d_{\mathrm{sed,max}}$, respectively. The sediment distributions for $d_{\mathrm{sed,mean}}$ are shown in Fig. 2, and S2 to S4 for the Clough-Tocher, nearest-neighbor, piecewise-linear, and ordinary kriging interpolation method, respectively.

IRD estimate [km^3]	Clough-Tocher	nearest-neighbor	piecewise-linear	ordinary kriging
average	753	939	800	916
min	187	226	212	216
max	1646	2078	1732	2071
Heinrich Layer 1	930	952	793	936
Heinrich Layer 2	1325	1268	1089	1255
Heinrich Layer 3	312	464	291	709
Heinrich Layer 4	725	1068	718	1143
Heinrich Layer 5	453	613	485	607
Heinrich Layer 6	199	281	139	173

When using the Clough-Tocher interpolation scheme, the estimates for individual HEs vary between 199 km^3 for Heinrich Layer 6 and 1325 km^3 for Heinrich Layer 2 (Table S1). In contrast to the results for an average Heinrich Layer, the ordinary kriging and nearest-neighbor methods lead to smaller estimates for Heinrich Layer 2 (1255 km^3 and 1268 km^3, respectively), indicating large differences in sediment discharge volume estimates of individual Heinrich Layers between interpolation methods. The piecewise-linear interpolation yields the overall smallest estimate of 139 km^3 (Heinrich Layer 6) and a maximum of 1089 km^3 for Heinrich Layer 2. Analyzing each Heinrich Layer separately can lead to smaller estimates than the ones based on the minimum estimates for an average Heinrich Layer because not all cores provide a sediment thickness estimate for each layer (e.g., only ~ 19 % of the 36 cores provide estimates for Heinrich Layer 6).

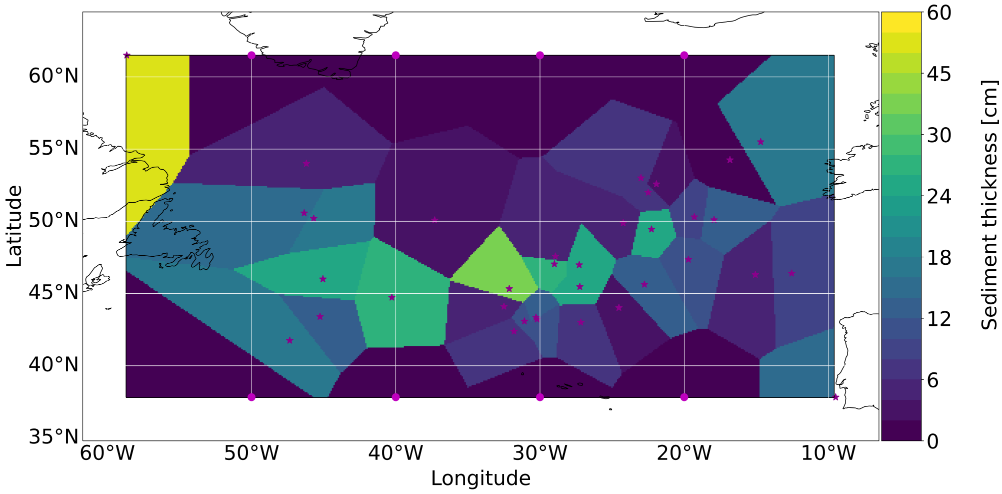

Fig. S2 Sediment thickness distribution based on the nearest-neighbor interpolation. Otherwise as Fig. 2.

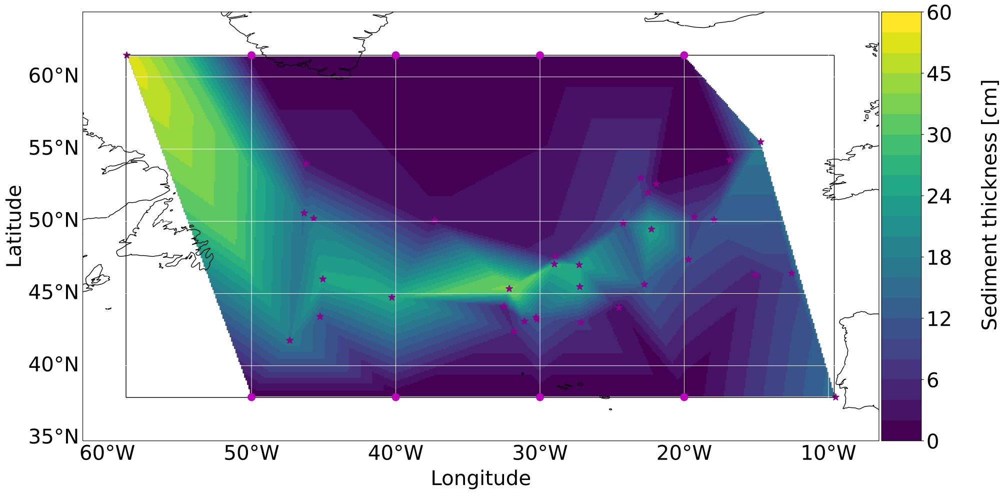

Fig. S3 Sediment thickness distribution based on the piecewise-linear interpolation. Otherwise as Fig. 2.

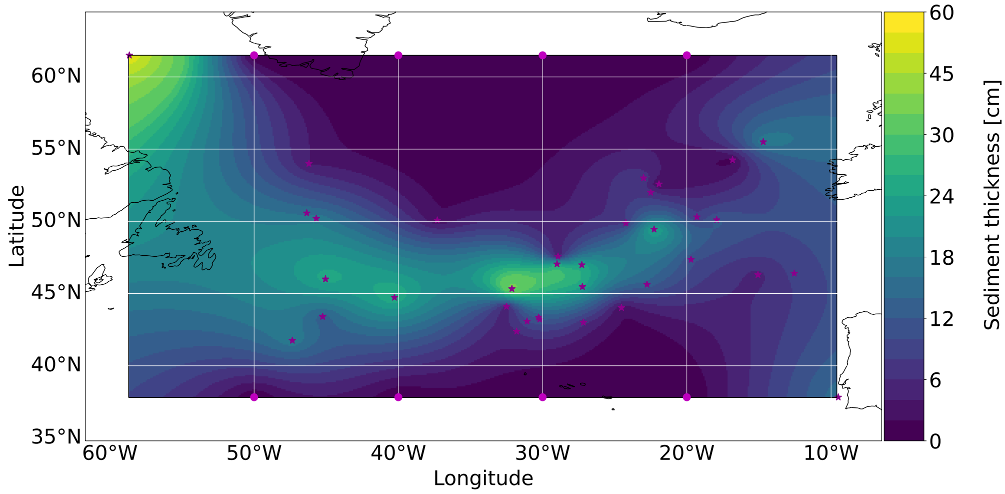

Fig. S4 Sediment thickness distribution based on the ordinary kriging interpolation. Otherwise as Fig. 2.

69 # S3 Correlation between freshwater and sediment flux

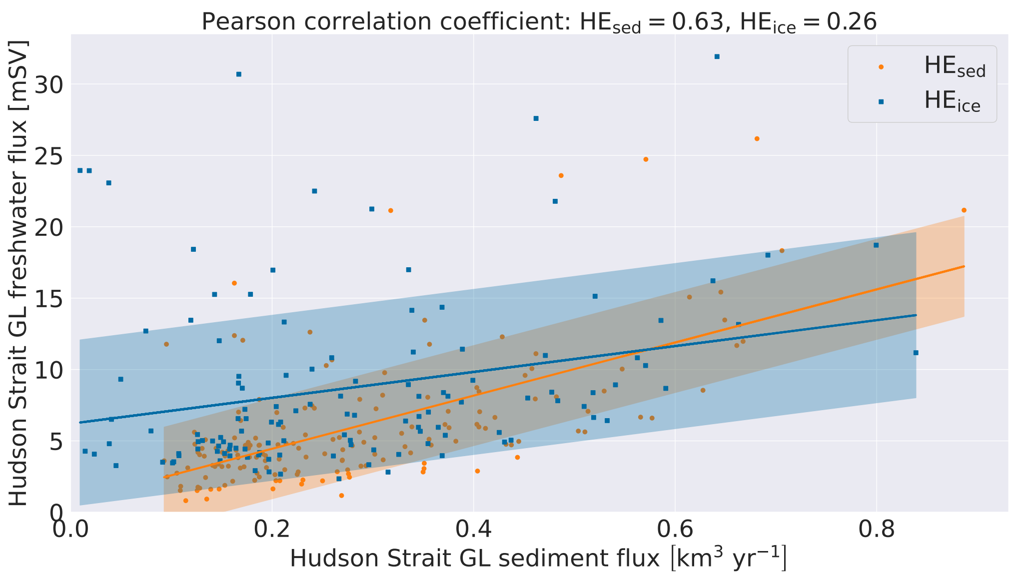

Fig. S5 Correlation between the Hudson Strait grounding line (GL) freshwater and sediment flux for all HE_{sed} (orange circles; 163 events) and HE_{ice} (blue squares; 126 events) across the 21 reference ensemble members. The orange/blue line and shaded area show the best fit and its standard deviation.

S4 Englacial sediment density

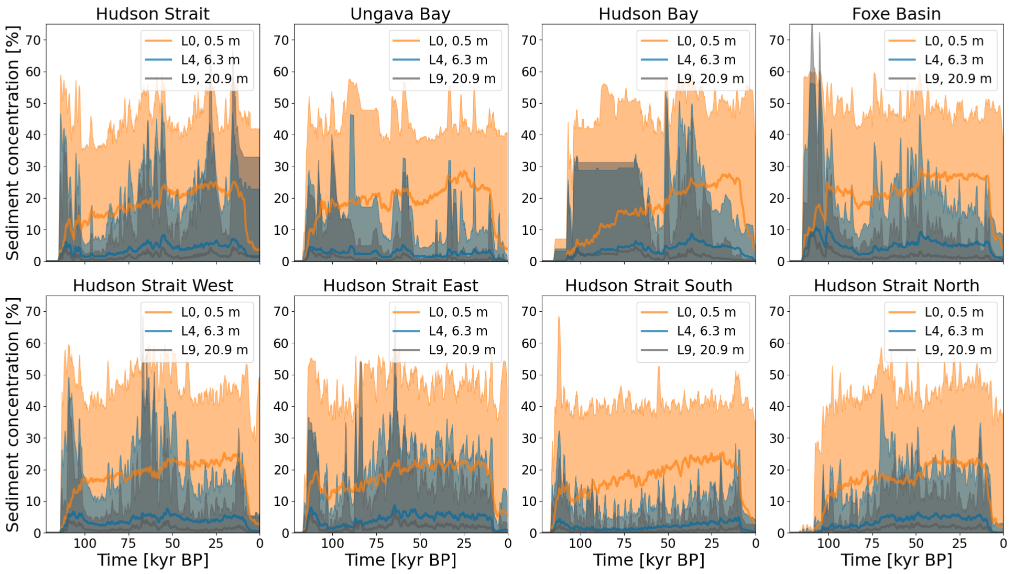

Fig. S6 Englacial sediment concentrations within 3 different layers of the sediment model. The thick lines represent the reference ensemble mean of the different layers. The shaded areas mark the reference ensemble minimum and maximum of the corresponding layer. L0 and L9 represent the bottom and top layers, respectively. The second numbers denote the height of the center of each layer. The locations of the sediment stations are shown in Fig. S14.

S5 Increased sediment deposition near the ice sheet grounding line

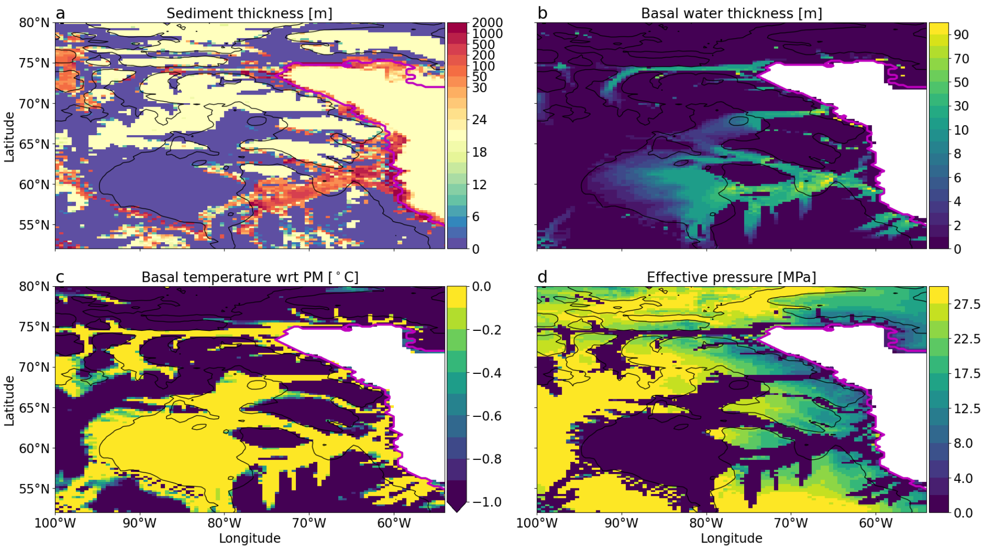

Fig. S7 Sediment thickness, basal water thickness, basal temperature with respect to the pressure melting point, and effective pressure for reference ensemble member 15 at 20 kyr BP. The initial sediment thickness is 20 m. The magenta and black contours show the grounding line and the present-day sea level (coastline) used in the GSM, respectively.

S6 Time series smoothing

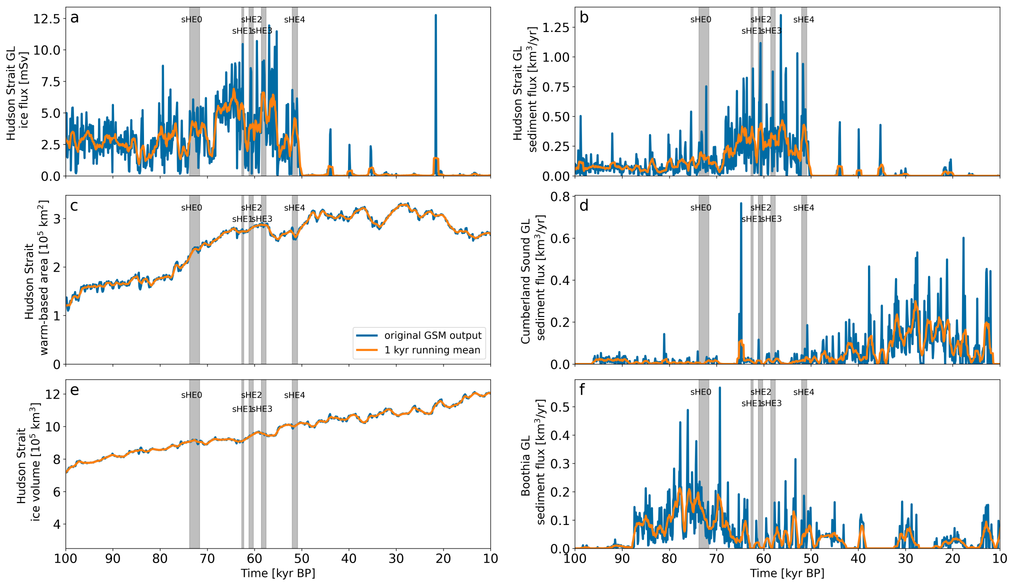

Fig. S8 Time series of reference ensemble member 19. The orange lines represent the time series used throughout this study (smoothed with 1 kyr running mean). The blue lines show the original GSM output (no smoothing). The shaded gray areas and black numbers mark the Hudson Strait HE_{sed} identified by the automated detection algorithm (Methods). The ice and sediment fluxes shown represent the respective flux across the grounding line (GL) within the corresponding areas in Fig. 4. The Hudson Strait warm-based area and ice volume are calculated within the Hudson Strait mask (Fig. 4).

S7 Sediment distribution

S7.1 Initial sediment distribution

A source of uncertainty when determining the sediment discharge volume during HEs is the poorly constrained sediment distribution across North America. Even for present-day, the sediment thickness estimates in, e.g., the Hudson Bay vary between < 5 and > 1500 m [e.g., Fig. 3 in 8]. Since the North American sediment distribution during the last interglacial (GSM initialization time) is even less constrained, we examine the effect of various uniform sediment distributions with an initial sediment thickness of $d_{\mathrm{sed,in}} = [0, 10, 20, 30, 40]$ m. Furthermore, two present-day sediment distributions ($d_{\mathrm{sed,PDlow}}$ and $d_{\mathrm{sed,PDhigh}}$ in Fig. S9) are used to bound model results within published estimates. While not necessarily representing unconsolidated deformable sediment, we use $d_{\mathrm{sed,PDhigh}}$ [9] as a maximum endmember scenario. Similarly, we use the sediment distribution based on the sediment cover map of [10, $d_{\mathrm{sed,PDlow}} = 100\,\mathrm{m} \cdot (\text{sediment cover})^5$; $0 \leq$ sediment cover ≤ 1] as a minimum endmember scenario. Except for isostatic adjustment due to replacing bedrock with sediment, the different initial sediment distributions retain the initial GSM topography (Fig. S1).

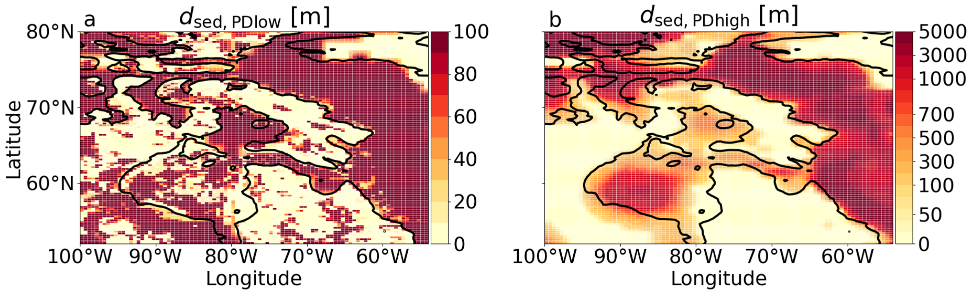

Fig. S9 Present-day endmember scenario sediment thickness distributions based on the sediment cover map of [10, panel a; $d_{\mathrm{sed,PDlow}} = 100$ m $\cdot$ (sediment cover)^5; $0 \leq$ sediment cover ≤ 1] and [9, panel b]. The black contour line shows the present-day sea level (coastline) used in the GSM. To prevent ice sheet growth over Greenland, the landmask in the corresponding area has been set to below sea level aside from a northwest Greenland stub to enable ice growth across Nares Strait.

In general, a thicker initial subglacial sediment thickness increases the ensemble mean englacial sediment thickness in Hudson Strait (Fig. S10a). However, the differences in mean englacial sediment thickness decrease with increasing initial sediment thickness. Due to the continuous evolution of the northeast American sediment distribution (e.g., Fig. S11), the variance in englacial sediment thickness across the ensemble increases, at times leading to overlapping mean englacial sediment thicknesses (60 to 40 kyr BP for $d_{\mathrm{sed,in}} = 20$ and 40 m in Fig. S10a). The ensemble mean Hudson Strait subglacial sediment thickness shows a similar and continuous increase over time for all initial sediment thicknesses (Fig. S10b).

Changes in ensemble ice and sediment flux characteristics due to different initial sediment thicknesses (shown for $\mathrm{HE_{ice}}$ and $\mathrm{HE_{sed}}$ in Fig. S12 and S13, respectively) are considered numerically significant when they exceed the **M**inimum **N**umerical **E**rror **E**stimates (MNEEs). MNEEs are determined for all ice and sediment flux characteristics based on their percentage difference between reference ensemble members and model runs with stricter numerical convergence thresholds [but otherwise the same parameters and model

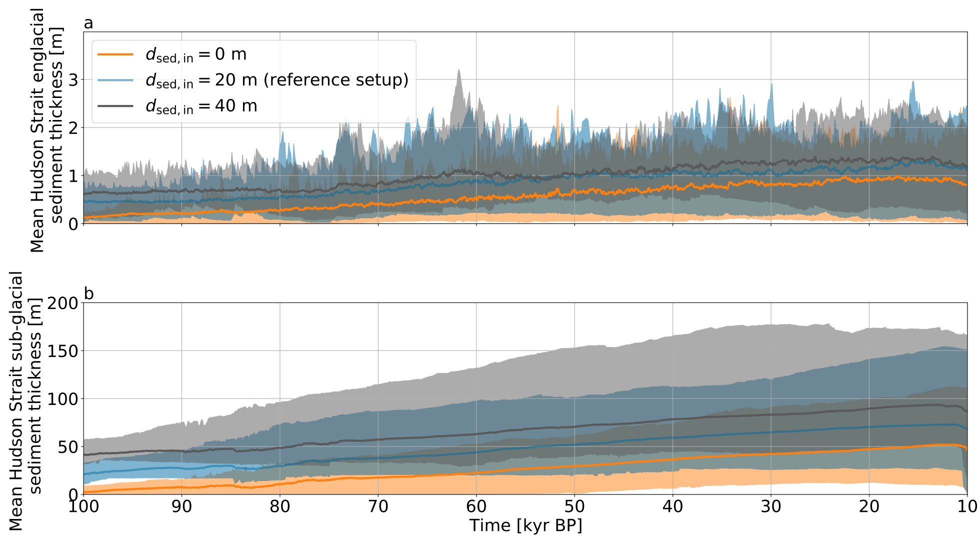

Fig. S10 Ensemble mean Hudson Strait englacial (a) and subglacial sediment thickness (b) for various uniform initial sediment thicknesses $d_{\mathrm{sed,in}}$. The thick lines represent the mean of the different ensembles (model setups). The shaded areas mark the minimum and maximum of the corresponding ensemble. The Hudson Strait area considered is outlined in Fig. 4. The time series are plotted without the 1 kyr running mean smoothing.

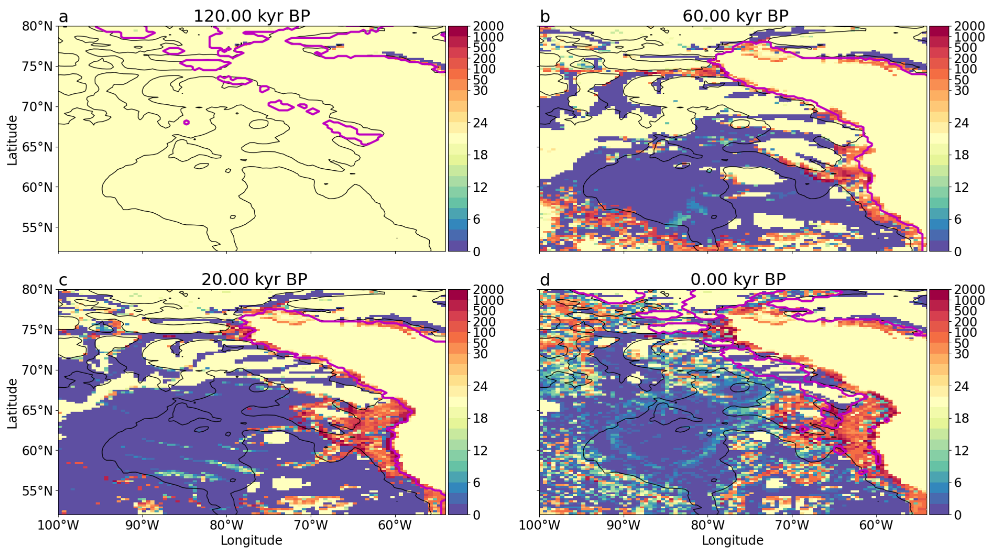

Fig. S11 Sediment thickness distribution across the eastern North American continent for reference ensemble member 19 in meters shown at different time steps. The initial sediment thickness is 20 m. The magenta and black contours show the grounding line and the present-day sea level (coastline) used in the GSM, respectively.

setup; 11, 12]. Differences smaller than the MNEEs are considered numerically insignificant. However, that does not necessarily mean the differences have no physical relevance.

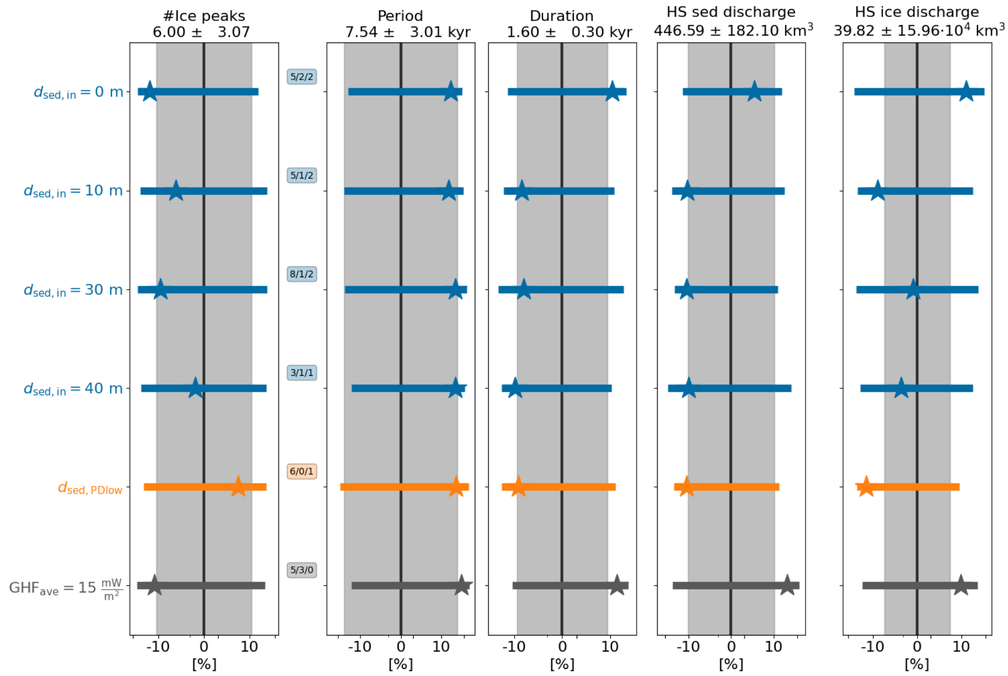

Fig. S12 Percentage differences in $\mathrm{HE_{ice}}$ ice and sediment flux characteristics compared to the GSM reference ensemble ($d_{\mathrm{sed,in}} = 20$ m). The shaded regions represent the MNEEs. HS sed discharge and HS ice discharge represent the sediment and ice discharge volume across the Hudson Strait (HS) grounding line during an $\mathrm{HE_{ice}}$, respectively. The different colors provide visual alignment of the individual comparison ensembles (model setups). The stars and horizontal bars are the ensemble mean percentage differences and standard deviations, respectively. The three numbers between the first and second column show the number of crashed model runs, the number of model runs without an $\mathrm{HE_{ice}}$, and the number of model runs with only one $\mathrm{HE_{ice}}$ in the comparison ensemble. The x-axes are logarithmic. The comparison ensembles, from top to bottom, are: $d_{\mathrm{sed,in}} = [0, 10, 30, 40]$ m, present-day sediment distribution based on the sediment cover map of [10, Fig. S9a], and average geothermal heat flux in Hudson Bay and Hudson Strait $\mathrm{GHF_{ave}} = 15\ \frac{\mathrm{mW}}{\mathrm{m}^2}$ [$d_{\mathrm{sed,in}} = 20$ m; 12]. Note that $d_{\mathrm{sed,in}}$ experiments with $\mathrm{GHF_{ave}} = 15\ \frac{\mathrm{mW}}{\mathrm{m}^2}$ lead to similar results (Fig. S19).

Except for the Hudson Strait ice discharge volume, the changes in $\mathrm{HE_{ice}}$ ice and sediment flux characteristics due to different initial sediment thicknesses are generally within the MNEEs (Fig. S12). Considering the standard deviations, the $\mathrm{HE_{ice}}$ characteristics are not significantly affected by the initial sediment distribution. Similarly, the $\mathrm{HE_{sed}}$ ice and sediment flux characteristics are not significantly affected by different initial sediment thickness distributions (Fig. S13). Note that all model runs with $d_{\mathrm{sed,PDhigh}}$ (Fig. S9b) crashed and the results are, therefore, not shown in Fig. S12 and S13. Based on the minor effects of the initial sediment thickness and the large uncertainties involved, we used the ensemble with medium uniform initial sediment thickness $d_{\mathrm{sed,in}} = 20$ m as our reference ensemble.

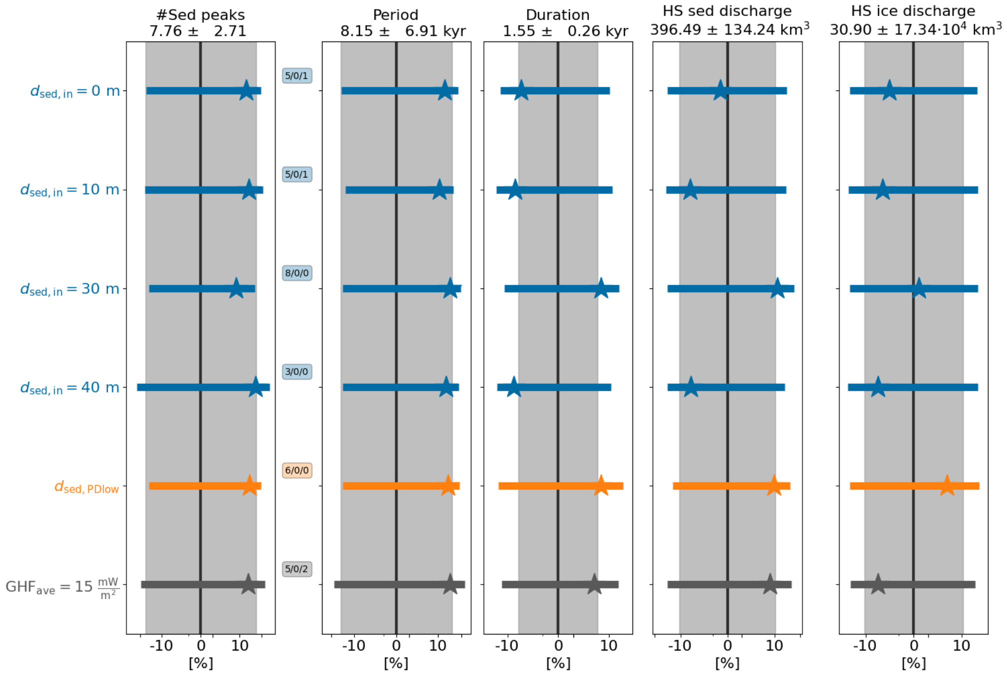

Fig. S13 Percentage differences in $\mathrm{HE}_{\mathrm{sed}}$ ice and sediment flux characteristics compared to the reference ensemble ($d_{\mathrm{sed,in}} = 20$ m). Otherwise as Fig. S12. Note that $d_{\mathrm{sed,in}}$ experiments with $\mathrm{GHF}_{\mathrm{ave}} = 15\ \frac{\mathrm{mW}}{\mathrm{m}^2}$ lead to similar results (Fig. S20).

S7.2 Northeast American sediment distribution

The present-day sediment distribution in the GSM model runs is generally within the bounds set by literature estimates [e.g., compare Fig. S11 and Fig. 3 in 8]. However, due to the large uncertainties associated with the present-day sediment distribution (differences > 1500 m), a more precise/detailed validation of the spatial distribution is currently not possible.

Due to sediment production by abrasion and quarrying as well as sub- and englacial sediment transport, the northeast American sediment distribution evolves continuously over the last glacial cycle. The sediment thickness on topographic highs remains relatively unchanged due to the generally low basal temperatures (lack of sedimentary processes under cold-based ice, e.g., Fig. S11). The largest differences occur within warm-based topographic troughs and along the ice sheet margin, where effective pressures are low and basal temperatures high (Eqs. 4 and 5).

The Hudson Bay and the catchment basins of other ice streams generally experience a decrease in subglacial sediment thickness (e.g., Fig. S11). Due to the prevailing basal water thickness, effective pressure, and basal melt rate in these areas, sediment entrainment and transport out of the region outweigh sediment production and melt-out (Fig. S7). The removed subglacial sediment then accumulates further downstream in the Hudson Strait, Cumberland Sound, and Boothia ice streams as well as along the Canadian coast.

Depending on the reference ensemble member in question, the sediment thickness at the Hudson Strait mouth can exceed 2 km by the end of the model run, which is within the large bounds provided by the published estimates. While coupling the GSM to an ocean-iceberg model is beyond the scope of this study, it would decrease the amount of locally deposited sediment along the ice sheet margin by distributing it across the North Atlantic.

S7.3 Englacial sediment distribution

On the modeling side, a key challenge for improving the understanding of HEs is that processes related to sediment erosion, entrainment, and deposition, as well as iceberg melt processes, are generally highly parameterized in numerical models, involving large parametric uncertainties [e.g., 8, 13, 14]. For example, there is no consensus on the englacial sediment distribution, including the limits of englacial sediment thickness terrestrial ice can transport. The maximum sediment thickness in a frozen-fringe model is 15 m [13]. In contrast, results of a coupled ocean-iceberg model indicate that icebergs with an isolated basal sediment layer cannot reproduce the observed Heinrich Layer distribution, even when considering capsized icebergs [14]. The authors conclude that sediment needs to be distributed throughout the entire volume of a 260 m thick iceberg to capture the sediment distribution pattern of a Heinrich Layer.

Here, we examine the sediment distribution within the ice column for 8 diagnostic locations along and across the Hudson Strait ice stream (Fig. S14). In general, the englacial sediment thickness during the last glacial cycle increases until deglaciation (Fig. S6). The sediment concentration is highest in the basal layer and continuously decreases towards higher layers. However, due to the limited total englacial sediment height in the model (23 m, Eq. 1), sediment can accumulate in the uppermost layer, and the concentration, at times, can then be higher than that of some lower layers.

During the initial ice sheet growth (first ~ 20 kyr BP of the model runs), the Hudson Strait ice stream (warm-based area and flow initiation) propagates from Hudson Strait mouth further upstream (e.g., Fig. S15). Therefore, sediment stations located further upstream show a delayed increase in englacial sediment concentration (from Hudson Strait

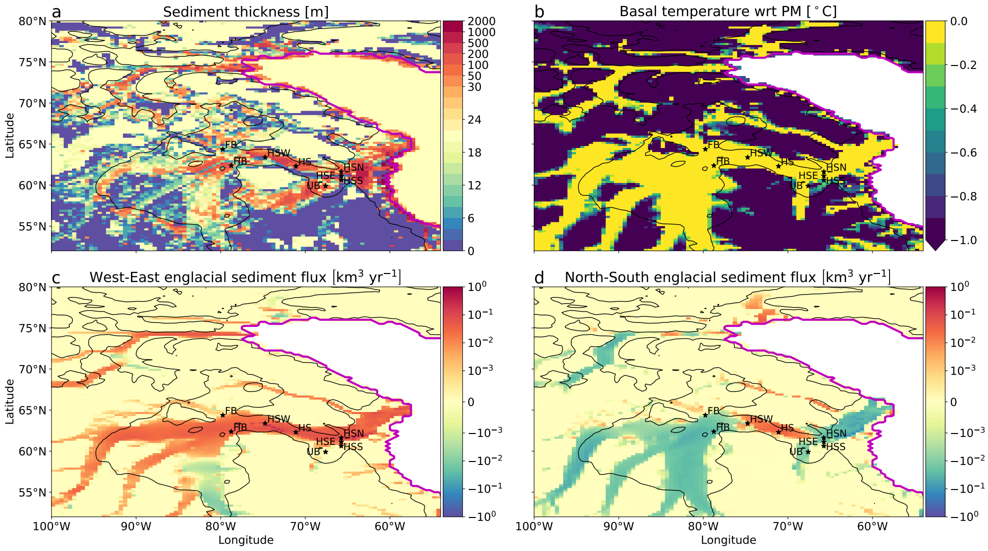

Fig. S14 Modeled output fields for reference ensemble member 12, all at 20 kyr BP. Sediment thickness (a), basal temperature with respect to the pressure melting point (b), West to East englacial sediment flux (c), and North to South englacial sediment flux (d). The initial sediment thickness is 20 m. The black asterisks mark the sediment stations for which the englacial sediment concentration is examined (Fig. S6 and S16): Hudson Bay (HB), Foxe Basin (FB), Hudson Strait West (HSW), Hudson Strait (HS), Ungava Bay (UB), Hudson Strait East (HSE), Hudson Strait South (HSS), Hudson Strait North (HSN). The magenta and black contours show the grounding line and the present-day sea level (coastline) used in the GSM, respectively.

East to Hudson Strait and then Hudson Strait West; Fig. S16a). As time progresses, sediment entrainment is eventually balanced by englacial sediment transport and deposition due to sediment meltout (increased basal melt rate within ice stream). The englacial sediment concentration in the basal layer (0.5 m center height) generally stays between 20 and 25 % within the ice stream (Fig. S16a). Similarly, there is limited cross-flow variation of sediment concentration (Hudson Strait North, Hudson Strait, and Hudson Strait South in Fig. S16b).

Closer to the catchment region, the englacial sediment concentration in the basal layer is higher for the Foxe Basin outlet than for the Hudson Bay outlet (Fig. S16a). The Hudson Bay station, located in a narrow trough, is generally near the margin of the warm-based area (Fig. S14b). Depending on the reference ensemble member and time in question, the Hudson Bay station does not experience continuous sediment entrainment (sediment entrainment over cold-based areas [e.g., 13] is not yet included in the GSM). Conversely, the Foxe Basin station is situated well within the warm-based area, enabling continuous sediment entrainment and increased englacial sediment concentrations.

Overall, the englacial sediment concentration is highest within the basal layer (up to 60 %) and reduces significantly further up (Fig. S6). The top layer (20.9 m center height) has generally < 5 %. The englacial sediment distribution modeled in the GSM is consistent with sediment thickness and concentration studies [up to 20 m and 60 %, but the observed basal layers are extremely complex and variable, 15–18]. A constant 4 % sediment concentration throughout the whole ice column (or iceberg), as, e.g., postulated by [14], is very unlikely. Better constraints on the present-day sediment discharge out of ice streams with comparable glaciological conditions and high-quality data of the sediment distribution within icebergs are required to improve sediment flux estimates during HEs.

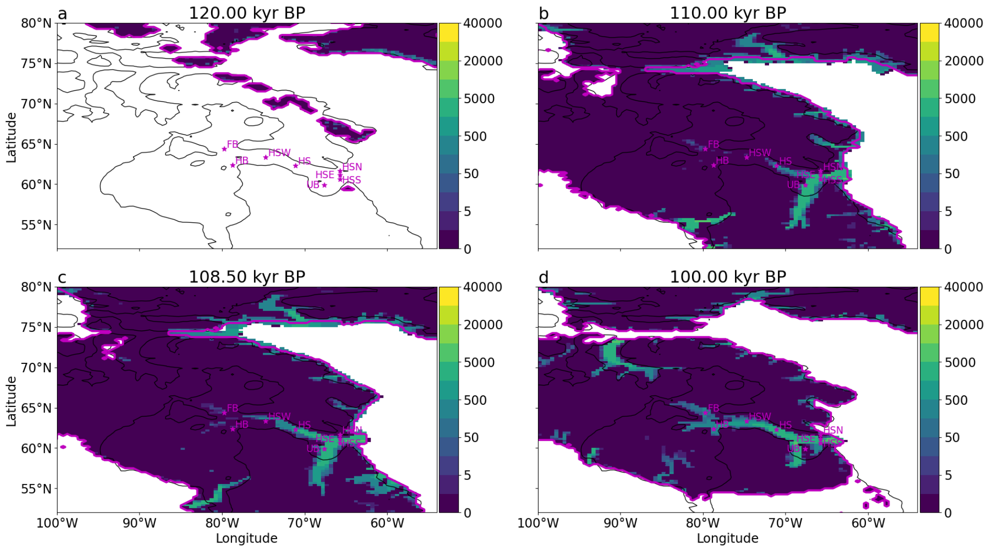

Fig. S15 Basal ice speed $\left[\mathrm{m\ yr^{-1}}\right]$ across the eastern North American continent for reference ensemble member 3 shown at different time steps. The magenta asterisks mark the sediment stations for which the englacial sediment concentration is examined (Fig. S14). The magenta and black contours show the grounding line and the present-day sea level (coastline) used in the GSM, respectively.

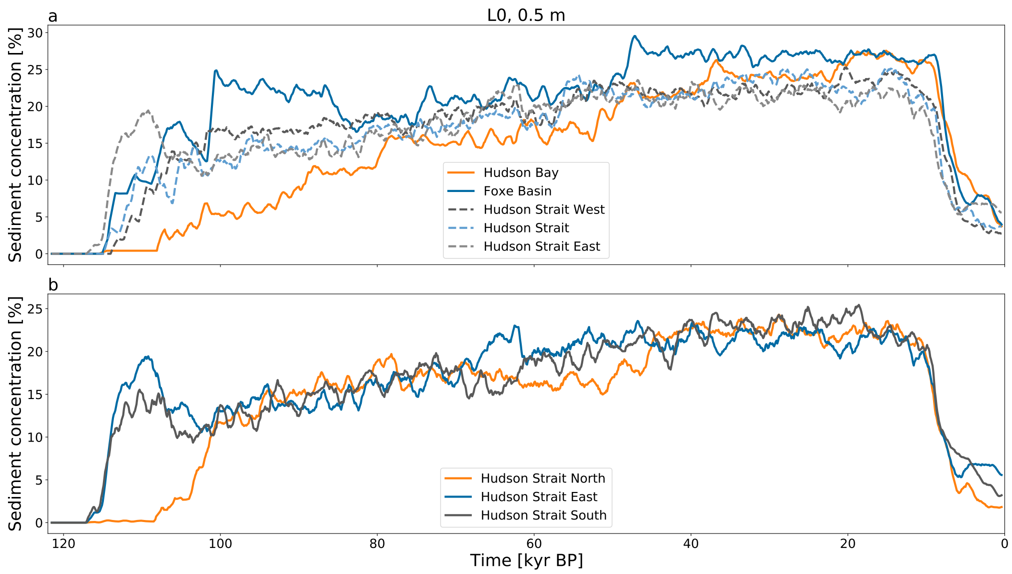

Fig. S16 Englacial sediment concentrations within the bottom layer (L0, 0.5 m center height) for sediment stations along (a) and across the Hudson Strait ice stream (b). All lines represent the reference ensemble mean per station. The exact locations of the sediment stations are shown in Fig. S14.

S8 Sediment discharge from northeast American ice streams

As Paleozoic carbonate is widespread in eastern Canada and ice streams can draw sediments from the same sedimentary basin (e.g., Hudson Strait and Cumberland Sound ice stream in Fig. S14c,d), we examine the sediment discharge volume of the Hudson Strait, Cumberland Sound, and Boothia ice stream during identified Hudson Strait HE_{sed}. Across the reference ensemble, the Hudson Strait sediment discharge volume (394 ± 134 km^3) is an order of magnitude larger than the Cumberland Sound and Boothia sediment discharge volume (34 ± 27 km^3 and 53 ± 23 km^3, respectively; Table S2).

Synchronized sediment flux peaks across the grounding line of the Hudson Strait, Cumberland Sound, and Boothia ice stream, as previously postulated for surges of the Mackenzie and Hudson ice stream [19], are scarce and show no indication of an interconnected system (e.g., Fig. S17b,d,f). The rare synchronous sediment flux peaks (e.g., sHE6 for Hudson Strait and Boothia ice stream in Fig. S17b,f) are, therefore, likely a coincidence.

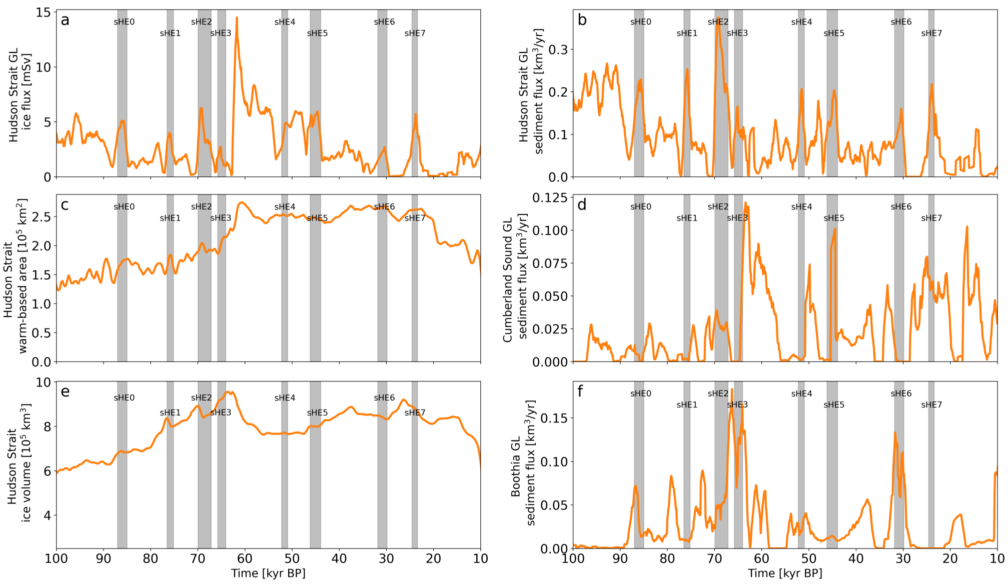

Fig. S17 Time series of reference ensemble member 6. Otherwise as Fig. S8.

S9 Ice and sediment flux characteristics for a lower geothermal heat flux

As discussed in detail in [12], a lower geothermal heat flux (GHF) leads to the classic binge-purge surge pattern of the Hudson Strait ice stream (e.g., Fig. S18a). Since neither a near continuous ice stream with pre-Heinrich Event shutdowns nor the classic binge-purge mechanism can be ruled out, we also examine the ice and sediment flux characteristics for a lower GHF (average GHF in Hudson Bay and Hudson Strait $GHF_{ave} = 15\ \frac{mW}{m^2}$, default is $GHF_{ave} \approx 70\ \frac{mW}{m^2}$). The differences in ice and sediment flux characteristics are generally within the MNEEs (Figs. S12 and S13) and as for the default GHF, different initial sediment thicknesses have generally no significant effect on the ice and sediment flux characteristics (Table S2; Figs. S19 and S20)

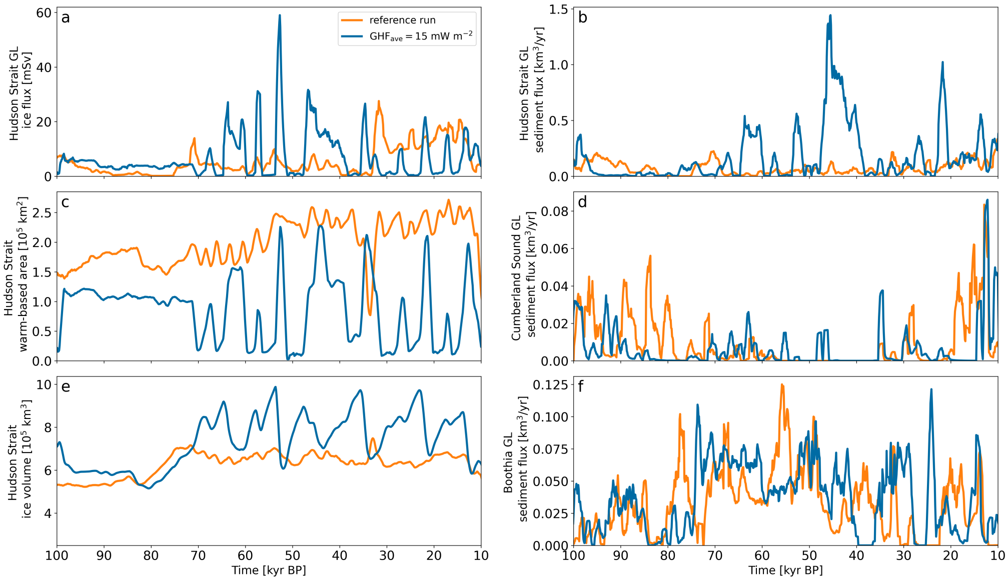

Fig. S18 Time series of reference ensemble member 1 ($GHF_{ave} \approx 70\ \frac{mW}{m^2}$) and a model run with lower GHF in the Hudson Strait and Hudson Bay ($GHF_{ave} = 15\ \frac{mW}{m^2}$). The Hudson Strait HE_{sed} are not highlighted for clarity. Otherwise as Fig. S8.

Table S2 HE_{sed} ice and sediment flux characteristics of the GSM reference ensemble compared to an ensemble with a lower geothermal heat flux in the Hudson Bay/Hudson Strait [12] and published estimates (all between 100 kyr BP and 10 kyr BP). The HE_{sed} characteristics are presented as mean ± standard deviation across all ensemble members.

Metric	reference ensemble	$GHF_{ave} = 15\ \frac{mW}{m^2}$ ensemble	literature estimates
number of HE_{sed}	7.8 ± 2.7	8.4 ± 4.7	6 to 10 [Table 6.3 in 20]
period [kyr]	8.2 ± 6.9	9.2 ± 5.1	4 to 15, mean= 8.0 ± 2.7 [Table 6.3 in 20]
duration [kyr]	1.6 ± 0.3	1.6 ± 0.3	0.2 to 2.3 [1]
Hudson Strait ice discharge volume [10^4 km^3]	31 ± 17	28 ± 16	-
Cumberland Sound ice discharge volume [10^4 km^3]	3 ± 2	2 ± 1	-
Boothia ice discharge volume [10^4 km^3]	4 ± 3	4 ± 2	-
total ice discharge volume [10^4 km^3]	~ 38	~ 34	3 to 946, , median= 75 [Table 1 in 21]
Hudson Strait sediment discharge volume [km^3]	396 ± 134	421 ± 174	-
Cumberland Sound sediment discharge volume [km^3]	34 ± 27	17 ± 9	-
Boothia sediment discharge volume [km^3]	53 ± 23	41 ± 18	-
total sediment discharge volume [km^3]	~ 483	~ 479	139 to 2078, average HE: 852 ± 78 (this study) 100 to 400 [1]

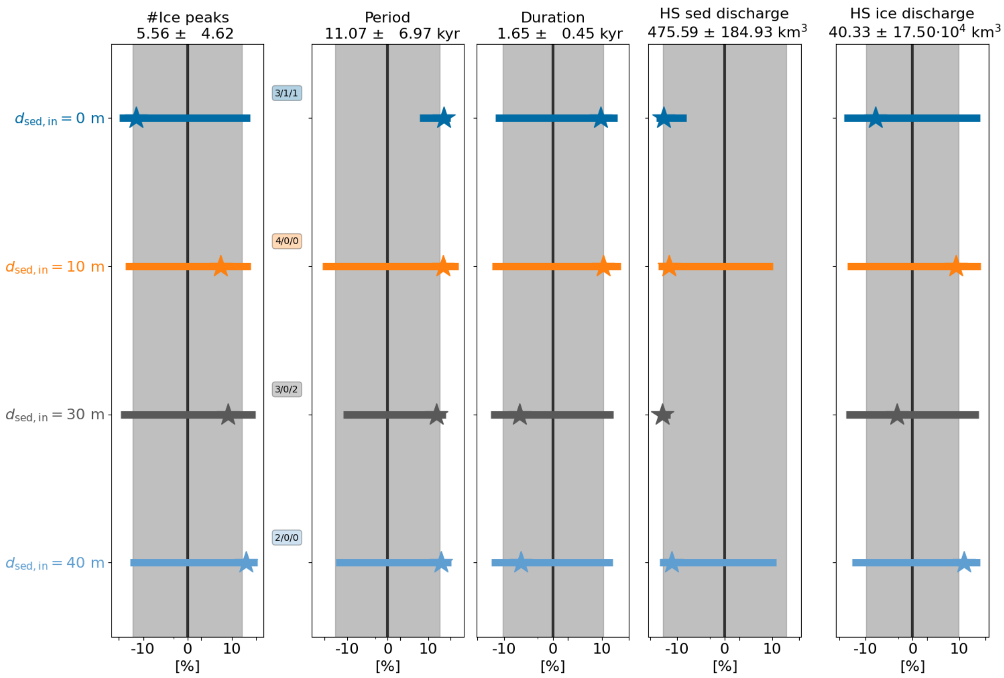

Fig. S19 Percentage differences in HE_{ice} ice and sediment flux characteristics compared to the $GHF_{ave} = 15\ \frac{mW}{m^2}$ ensemble (uniform initial sediment thickness $d_{sed,in} = 20$ m). All experiments, including the shown MNEEs, also use $GHF_{ave} = 15\ \frac{mW}{m^2}$ [12]. The comparison ensembles (model setups), from top to bottom, are: $d_{sed,in} = [0, 10, 30, 40]$ m. 6 (out of 21) $GHF_{ave} = 15\ \frac{mW}{m^2}$ ensemble members crashed and 3 members do not show HE_{ice}. The corresponding parameter vectors were not considered for the statistics shown here. Otherwise as Fig. S12.

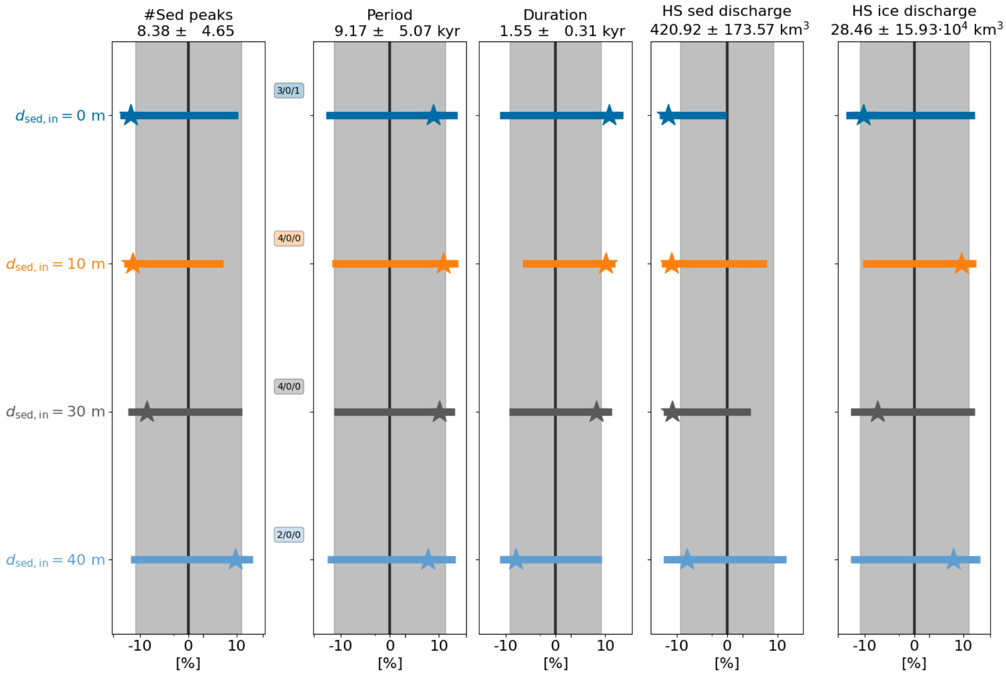

Fig. S20 Percentage differences in HE_{sed} ice and sediment flux characteristics compared to the $GHF_{ave} = 15\ \frac{mW}{m^2}$ ensemble (uniform initial sediment thickness $d_{sed,in} = 20$ m). All experiments, including the shown MNEEs, also use $GHF_{ave} = 15\ \frac{mW}{m^2}$ [12]. 6 (out of 21) $GHF_{ave} = 15\ \frac{mW}{m^2}$ ensemble members crashed and 3 members do not show HE_{ice}. The corresponding parameter vectors were not considered for the statistics shown here. Otherwise as Fig. S13.

S10 Effect of different relative heights in peak prominence algorithm

Table S3 Comparison of HE_{ice} ice and sediment flux characteristics (mean ± standard deviation) between 100 kyr BP and 10 kyr BP for the reference ensemble when using different relative heights H_{rel} in the peak prominence algorithm.

HE_{ice}	$H_{rel} = 0.25$	$H_{rel} = 0.50$ (reference)	$H_{rel} = 0.75$
number of events	6.8 ± 3.1	6.0 ± 3.1	3.3±2.3
period [kyr]	8.1 ± 3.6	7.5 ± 3.0	10.2 ± 6.2
duration [kyr]	1.0 ± 0.2	1.6 ± 0.3	1.9 ± 0.3
ice discharge volume [10^4 km^3]	25 ± 8	40 ± 16	47 ± 18
freshwater flux [mSv]	9 ± 4	8 ± 4	8 ± 4
sediment discharge volume [km^3]	257 ± 107	447 ± 182	560 ± 300

Table S4 Comparison of HE_{sed} ice and sediment flux characteristics (mean ± standard deviation) between 100 kyr BP and 10 kyr BP for the reference ensemble when using different relative heights H_{rel} in the peak prominence algorithm.

HE_{sed}	$H_{rel} = 0.25$	$H_{rel} = 0.50$ (reference)	$H_{rel} = 0.75$
number of events	5.9 ± 2.3	7.8 ± 2.7	5.6 ± 2.1
period [kyr]	9.8 ± 7.1	8.2 ± 6.9	9.8 ± 5.8
duration [kyr]	1.0 ± 0.1	1.6 ± 0.3	1.8 ± 0.4
ice discharge volume [10^4 km^3]	21 ± 7	31 ± 17	33 ± 17
freshwater flux [mSv]	7 ± 3	6 ± 3	6 ± 3
sediment discharge volume [km^3]	316 ± 89	396 ± 134	409 ± 143

References

[1] Hemming, S.: Heinrich events: Massive late Pleistocene detritus layers of the North Atlantic and their global climate imprint. Reviews of Geophysics - REV GEOPHYS **42**(1) (2004) https://doi.org/10.1029/2003RG000128

[2] Virtanen, P., Gommers, R., Oliphant, T.E., Haberland, M., Reddy, T., Cournapeau, D., Burovski, E., Peterson, P., Weckesser, W., Bright, J., Walt, S.J., Brett, M., Wilson, J., Millman, K.J., Mayorov, N., Nelson, A.R.J., Jones, E., Kern, R., Larson, E., Carey, C.J., Polat, I., Feng, Y., Moore, E.W., VanderPlas, J., Laxalde, D., Perktold, J., Cimrman, R., Henriksen, I., Quintero, E.A., Harris, C.R., Archibald, A.M., Ribeiro, A.H., Pedregosa, F., Mulbregt, P., Vijaykumar, A., Bardelli, A.P., Rothberg, A., Hilboll, A., Kloeckner, A., Scopatz, A., Lee, A., Rokem, A., Woods, C.N., Fulton, C., Masson, C., Häggström, C., Fitzgerald, C., Nicholson, D.A., Hagen, D.R., Pasechnik, D.V., Olivetti, E., Martin, E., Wieser, E., Silva, F., Lenders, F., Wilhelm, F., Young, G., Price, G.A., Ingold, G.-L., Allen, G.E., Lee, G.R., Audren, H., Probst, I., Dietrich, J.P., Silterra, J., Webber, J.T., Slavič, J., Nothman, J., Buchner, J., Kulick, J., Schönberger, J.L., de Miranda Cardoso, J.V., Reimer, J., Harrington, J., Rodríguez, J.L.C., Nunez-Iglesias, J., Kuczynski, J., Tritz, K., Thoma, M., Newville, M., Kümmerer, M., Bolingbroke, M., Tartre, M., Pak, M., Smith, N.J., Nowaczyk, N., Shebanov, N., Pavlyk, O., Brodtkorb, P.A., Lee, P., McGibbon, R.T., Feldbauer, R., Lewis, S., Tygier, S., Sievert, S., Vigna, S., Peterson, S., More, S., Pudlik, T., Oshima, T., Pingel, T.J., Robitaille, T.P., Spura, T., Jones, T.R., Cera, T., Leslie, T., Zito, T., Krauss, T., Upadhyay, U., Halchenko, Y.O., Vázquez-Baeza, Y., Contributors, S...: SciPy 1.0: fundamental algorithms for scientific computing in Python. Nature Methods **17**(3), 261–272 (2020) https://doi.org/10.1038/s41592-019-0686-2

[3] Murphy, B., Yurchak, R., Müller, S.: GeoStat-Framework/PyKrige: v1.7.2. Zenodo (2024). https://doi.org/10.5281/zenodo.11360184 . https://doi.org/10.5281/zenodo.11360184

[4] Veiga-Pires, C.C., Hillaire-Marcel, C.: U and Th isotope constraints on the duration of Heinrich events H0-H4 in the southeastern Labrador Sea. Paleoceanography **14**(2), 187–199 (1999) https://doi.org/10.1029/1998PA900003

[5] Gibb, O.T., Hillaire-Marcel, C., Vernal, A.: Oceanographic regimes in the northwest Labrador Sea since Marine Isotope Stage 3 based on dinocyst and stable isotope proxy records. Quaternary Science Reviews **92**, 269–279 (2014) https://doi.org/10.1016/j.quascirev.2013.12.010

[6] Hesse, R., Khodabakhsh, S.: Anatomy of Labrador Sea Heinrich layers. Marine Geology **380**, 44–66 (2016) https://doi.org/10.1016/j.margeo.2016.05.019

[7] McKay, R., Albot, O., Dunbar, G.B., Lee, J.I., Lee, M.K., Yoo, K.C., Kim, S., Turton, N., Kulhanek, D., P̃atterson, M., Levy, R.: A Comparison of Methods for Identifying and Quantifying Ice Rafted Debris on the Antarctic Margin. Paleoceanography and Paleoclimatology **37**(4) (2022) https://doi.org/10.1029/2021PA004404

[8] Drew, M., Tarasov, L.: North American Pleistocene Glacial Erosion and Thin Pliocene Regolith Thickness Inferred from Data-Constrained Fully Coupled Ice-Climate-Sediment modelling. EGUsphere **2024**, 1–50 (2024) https://doi.org/10.5194/

egusphere-2024-620

[9] Laske, G., Masters, G.: A global digital map of sediment thickness. EOS Trans. **78**, 483 (1997)

[10] Geological Survey of Canada: Surficial Geology of Canada / Géologie des Formations Superficielles du Canada. Natural Resources Canada. Open Access (2014). https://doi.org/10.4095/295462 . https://doi.org/10.4095/295462

[11] Hank, K., Tarasov, L., Mantelli, E.: Modeling sensitivities of thermally and hydraulically driven ice stream surge cycling. Geoscientific Model Development **16**(19), 5627–5652 (2023) https://doi.org/10.5194/gmd-16-5627-2023

[12] Hank, K., Tarasov, L.: The comparative role of physical system processes in Hudson Strait ice stream cycling: a comprehensive model-based test of Heinrich event hypotheses. Climate of the Past **20**(11), 2499–2524 (2024) https://doi.org/10.5194/cp-20-2499-2024

[13] Meyer, C.R., Robel, A.A., Rempel, A.W.: Frozen fringe explains sediment freeze-on during Heinrich events. Earth and Planetary Science Letters **524**, 115725 (2019) https://doi.org/10.1016/j.epsl.2019.115725

[14] Fendrock, M., Condron, A., McGee, D.: Modeling the Production of Heinrich Layers With a Sediment-Enabled Iceberg Model. Paleoceanography and Paleoclimatology **38**(6), 1–12 (2023) https://doi.org/10.1029/2022pa004583

[15] Herron, S., Hoar, Langway, C.C.: The Debris-Laden Ice at the Bottom of the Greenland Ice Sheet. Journal of Glaciology **23**(89), 193–207 (1979) https://doi.org/10.3189/S002214300002983X

[16] Dowdeswell, J.A., Dowdeswell, E.K.: Debris in icebergs and rates of glaci-marine sedimentation: observations from Spitsbergen and a simple model. Journal of Geology **97**(2), 221–231 (1989) https://doi.org/10.1086/629296

[17] Lawson, D.E., Strasser, J.C., Evenson, E.B., Alley, R.B., Larson, G.J., Arcone, S.A.: Glaciohydraulic supercooling: a freeze-on mechanism to create stratified, debris-rich basal ice: I. field evidence. Journal of Glaciology **44**(148), 547–562 (1998) https://doi.org/10.3189/S0022143000002069

[18] Knight, P.G., Patterson, C.J., Waller, R.I., Jones, A.P., Robinson, Z.P.: Preservation of basal-ice sediment texture in ice-sheet moraines. Quaternary Science Reviews **19**(13), 1255–1258 (2000) https://doi.org/10.1016/S0277-3791(00)00091-3

[19] Schannwell, C., Mikolajewicz, U., Ziemen, F., Kapsch, M.-L.: Sensitivity of Heinrich-type ice-sheet surge characteristics to boundary forcing perturbations. Climate of the Past **19**(1), 179–198 (2023) https://doi.org/10.5194/cp-19-179-2023

[20] Bradley, R.: Paleoclimatology (3rd Edition), (2014)

[21] Roberts, W.H.G., Valdes, P.J., Payne, A.J.: A new constraint on the size of Heinrich Events from an iceberg/sediment model. Earth and Planetary Science Letters **386**, 1–9

(2014) https://doi.org/10.1016/j.epsl.2013.10.020